

THE HISTORY OF STAR FORMATION IN GALAXY DISKS IN THE LOCAL VOLUME AS MEASURED BY THE ACS NEARBY GALAXY SURVEY TREASURY

BENJAMIN F. WILLIAMS¹, JULIANNE J. DALCANTON¹, L. C. JOHNSON¹, DANIEL R. WEISZ¹, ANIL C. SETH^{2,7}, ANDREW DOLPHIN³, KAROLINE M. GILBERT^{1,8}, EVAN SKILLMAN⁴, KEITH ROSEMA⁴, STEPHANIE M. GOGARTEN¹, JON HOLTZMAN⁵, ROELOF S. DE JONG⁶,

Draft version July 5, 2018

ABSTRACT

We present a measurement of the age distribution of stars residing in spiral disks and dwarf galaxies. We derive a complete star formation history of the ~ 140 Mpc³ covered by the volume-limited sample of galaxies in the Advanced Camera for Surveys (ACS) Nearby Galaxy Survey Treasury (ANGST). The total star formation rate density history ($\rho_{SFR}(t)$) is dominated by the large spirals in the volume, although the sample consists mainly of dwarf galaxies. Our $\rho_{SFR}(t)$ shows a factor of ~ 3 drop at $z \sim 2$, in approximate agreement with results from other measurement techniques. While our results show that the overall $\rho_{SFR}(t)$ has decreased since $z \sim 1$, the measured rates during this epoch are higher than those obtained from other measurement techniques. This enhanced recent star formation rate appears to be largely due to an increase in the fraction of star formation contained in low-mass disks at recent times. Finally, our results indicate that despite the differences at recent times, the epoch of formation of $\sim 50\%$ of the stellar mass in dwarf galaxies was similar to that of $\sim 50\%$ of the stellar mass in large spiral galaxies ($z \gtrsim 2$), despite the observed galaxy-to-galaxy diversity among the dwarfs.

Subject headings: galaxies: stellar content — galaxies: evolution

1. INTRODUCTION

The star formation history of the universe ($\rho_{SFR}(t)$) constrains models of structure formation, the assembly of galaxies, metal production, and the epoch of reionization. Currently there are testable models for the growth of structure in the universe on all scales, for the flow of gas in and out of galaxies, and the conversion of gas into stars. If these models are correct, then we should expect consistency between the models and observations of the rate at which galaxies formed stars throughout cosmic time at all galaxy mass scales. Moreover, we should expect a similar level of consistency between the observed *in situ* star formation rate (SFR) and the stellar record and metal content of the universe at the present day.

With the combination of *HST*, large aperture redshifts surveys, and well-calibrated photometric redshifts, there has been an explosion of observational constraints on the SFR at high redshifts (e.g. Madau et al. 1996; Connolly et al. 1997; Lilly et al. 1996; Steidel et al. 1999;

Fontana et al. 2003; Iwata et al. 2003; Bunker et al. 2004; Giavalisco et al. 2004), now pushing out to $z \gtrsim 8$ (Bouwens et al. 2010). These measurements have been augmented by measurements of the obscured SFR due to advances in the capabilities of long wavelength detectors allowing measurements of high- z star formation (Chapman et al. 2005). Such assessment of the SFR has also been made at low redshifts by surveys like the Sloan Digital Sky Survey (SDSS Heavens et al. 2004) and the Galaxy Evolution Explorer (GALEX Schiminovich et al. 2005) all on the basic properties of SFR versus time.

While early measurements of $\rho_{SFR}(t)$ showed a peak around $z \sim 1.5$ (e.g. Madau et al. 1996; Connolly et al. 1997; Hopkins et al. 2001), more recent measurements have generally put the peak prior to $z \sim 2$ (e.g. Lanzetta et al. 2002; Hopkins 2004; Chapman et al. 2005; Bouwens et al. 2007; Reddy et al. 2008), including measurements combining the star formation histories (SFHs) of Local Group galaxies. Inside the LG Hopkins et al. (2001) found that $\rho_{SFR}(t)$ was broadly consistent with redshift surveys with no significant contribution from dwarfs at any epoch, and Drozdovsky et al. (2008) found an excess of star formation in recent epochs, dominated by the disk of the Milky Way, as well as a recent increase in the contribution from dwarfs. Weisz et al. (2011b) found little difference in the SFHs of the LG dwarfs and those in a larger volume. Only one recent measurement, based on integrated galaxy spectra in the Sloan Digital Sky Survey (Heavens et al. 2004), has found a peak more recent than $z = 2$. Furthermore, recent analytical calculations (Hernquist & Springel 2003), semi-analytic galaxy formation models (Lacey et al. 2009), and hydrodynamic simulations (Springel & Hernquist 2003) also generally put the peak earlier than $z \sim 2$. For current WMAP cosmology, this places the peak at lookback times >10

¹ Department of Astronomy, Box 351580, University of Washington, Seattle, WA 98195; ben@astro.washington.edu; jd@astro.washington.edu; lcj@astro.washington.edu; dweisz@astro.washington.edu; kgilbert@astro.washington.edu; krosema@astro.washington.edu; stephanie@astro.washington.edu

² Harvard-Smithsonian Center for Astrophysics, 60 Garden Street, Cambridge, MA 02138; aseth@cfa.harvard.edu

³ Raytheon, 1151 E. Hermans Road, Tucson, AZ 85706; adolphin@raytheon.com

⁴ Department of Astronomy, University of Minnesota, 116 Church St. SE, Minneapolis, MN 55455; skillman@astro.umn.edu

⁵ Department of Astronomy, New Mexico State University, Box 30001, 1320 Frenger St., Las Cruces, NM 88003; holtz@nmsu.edu

⁶ Astrophysikalisches Institut Potsdam, Potsdam, Germany; rdejong@aip.de

⁷ CfA Fellow.

⁸ Hubble Fellow.

Gyr. There is mounting evidence that low-mass galaxies may have later formation times (i.e. “down-sizing” Cowie et al. 1996; Lilly et al. 2003; Thomas et al. 2005; Neistein et al. 2006, and many others), which could in principle affect the location of the $\rho_{SFR}(t)$ peak. Unfortunately, direct constraints at high redshift are challenging, given that all *in situ* redshift-based studies have magnitude limits that prohibit the inclusion of low-mass galaxies in their measurements.

Herein, we report our measurement $\rho_{SFR}(t)$ in our local volume using resolved stellar populations from a volume-limited sample of galaxy disks: the largest ever measured using resolved stellar populations analysis. Our approach has the benefit that we simultaneously explore the past SFH and the present stellar record. Moreover, we have complete, volume-limited sampling of the galaxy population down to very low masses, rather than the high-mass galaxies that dominate *in situ* high-redshift studies. The limitations of the approach are difficulty resolving stars in massive spheroids, so that we can only trace the SFH of disks and dwarf galaxies, and a relatively short distance over which stars can be resolved with *HST*, so that we cannot measure a truly representative volume of the universe. Our results are generally consistent with those of recent redshift surveys, and we conclude that with the currently-possible depth of resolved stellar photometry over this volume, we cannot resolve the age of the peak beyond placing it at $z > 2$.

2. DATA ACQUISITION, REDUCTION, AND ANALYSIS

All of the data for this study were analyzed through the ANGST (GO-10915) and ACS Nearby Galaxies: Reduce, Reuse, Recycle (ANGRRR; AR-10945) programs⁹. Our full sample is detailed in Table 1 and in Dalcanton et al. (2009). The motivation for the sample selection was to stay within a limited volume. We have included all galaxies inside of ~ 3.5 Mpc, but outside the LG (as defined by van den Bergh 2000, ~ 8 Mpc³) and more than 20° from the Galactic plane ($\sim 34\%$ of the sphere). ANGST extended this distance limit to ~ 4 Mpc in the direction of the M81 group and Sculptor filament to improve sampling of massive galaxies and dense environments. The Cen A group, which is also within ~ 4 Mpc, was excluded due to its low galactic latitude and incomplete galaxy census. Our sample therefore covers only $\sim 70\%$ of the stellar mass in the volume between 3.5 and 4.0 Mpc, making our effective distance limit ~ 3.8 Mpc. Therefore, our net volume surveyed is ~ 140 Mpc³. This scale is smaller than the large scale structure of the universe, and thus we may be sampling a non-representative environment. Therefore differences between our results and those of redshift surveys may be primarily due to such sampling effects.

We exclude KDG73 and Sc22 as their revised distance moduli place them beyond 4 Mpc, and we exclude BK6N and KKH57 due to poor data quality. The program obtained ACS and WFPC2 imaging of a volume-limited sample of galaxies. All photometry techniques are described in detail in Dalcanton et al. (2009) and K. Gilbert et al. (in preparation). In short, the photometry and artificial star tests were measured simultaneously for all of the objects in the uncombined images using the

software packages HSTPHOT and DOLPHOT (Dolphin 2000), and the output data were culled on signal-to-noise, sharpness, and crowding.

2.1. SFH Determination

We measured the SFR and metallicity as a function of stellar age using the software package MATCH (Dolphin 2002). We fit the observed CMDs (with magnitude cuts set to limits provided in Table 1) by populating the stellar evolution models of Girardi et al. (2002, with updates in Marigo et al. 2008; Girardi et al. 2010) with a Salpeter (1955) initial mass function (IMF). We fixed the distance and reddening to the Dalcanton et al. (2009) values. The best fit provides the relative contribution of stars of each age and metallicity in each field.

We then performed Monte Carlo fits by resampling the best-fitting model 100 times. Then, when fitting the realizations, the systematic errors are accounted for by introducing small random shifts in the bolometric magnitudes and effective temperatures of the models. These shifts are introduced at the level of the differences between models in the literature, and therefore serve as a proxy of the effects of our choice of stellar evolution models. From these tests we calculated our uncertainties due to Poisson sampling, errors in photometry, and systematic errors due to deficiencies in the stellar evolution models as well as any offset in distance, reddening, and/or zero-points.

Our time bins were chosen based on the features present in most of our data. In general, the main-sequence and blue He-burning sequences provide high resolution time sensitivity for times more recent than ~ 400 Myr. After this epoch, our photometry contains only the RGB, which contains degeneracies between age and metallicity (Gallart et al. 2005), and the AGB, which is generally poorly populated and suffers from poorly-constrained models (Melbourne et al. 2010), and the red clump, which is dominated by old ($\gtrsim 2$ Gyr) stars. We therefore limited ourselves to 4 bins in this large interval: one long bin on each side of ~ 1 Gyr ago (the epoch where our CMDs provide the least information) in order to leverage more reliable age information from before and after this period, and two more bins where we have additional information from the red clump to help constrain the age distribution (4–10 Gyr and 10–14 Gyr).

When determining the SFHs, we check the effects of our varying depth and magnitude cuts for fitting each CMD. Due to the failure of ACS during the ANGST program, our photometry sample is heterogeneous and of varying depth (see electronic Table 1). Nevertheless, the bulk of the stellar mass is in M81 and NGC253, which were both observed with ACS, and every attempt was made to obtain a depth reaching the red clump feature in the CMD with WFPC2 ($M_{F814W} \sim -0.3$, $M_{F606W} \sim 0.4$). Furthermore, our SFHs for ancient times (> 2 Gyr) were always taken from the deepest data available, which for most low-mass galaxies, included information from the red clump feature (see electronic Table 1 and Figure 1). There is still no guarantee that our data were all detailed enough to reliably separate populations with ages slightly less than 10 Gyr from those with ages slightly greater than 10 Gyr.

⁹ <http://www.nearbygalaxies.org/>

2.2. SFH Scaling

Our fields cover only a portion of each galaxy, making it necessary to scale the measured SFH to the total galaxy mass. Once we had measured the SFHs for the deepest available field in each ANGST galaxy, we renormalized the SFRs to a Kroupa (2002) IMF (divided by 2), and we scaled them to the total stellar mass in each galaxy. We first estimated the galaxy’s total stellar mass from *Spitzer* photometry (see below). The stellar mass contained in our ANGST field was then calculated directly from our SFH. The quotient of these provided our estimate of the fraction of the galaxy’s stellar mass contained in our field ($SFR_{total}(t) = SFR_{field}(t) \times \frac{M_{star,3.6\mu}}{M_{star,SFH}}$).

To estimate each galaxy’s total stellar mass, we used the total *Spitzer* 3.6 μ m luminosity from the *Spitzer* Local Volume Legacy Survey (Dale et al. 2009). To determine the appropriate $M/L_{3.6\mu}$ to apply, we calculated $M/L_{3.6\mu}$ using stellar masses determined by our CMD fits and *Spitzer* 3.6 μ photometry of the fields with good *Spitzer* coverage and minimal foreground contamination. In all cases with reliable *Spitzer* data covering our field, $M/L_{3.6\mu} = 0.5 \pm 0.2$. We therefore assumed $M/L_{3.6\mu} = 0.5$ to estimate each galaxy’s total stellar mass. We verified that this assumption resulted in a total stellar masses of M81 and NGC 253 less than the mass calculated from their rotation curves (as taken from Puche et al. 1991; Adler & Westpfahl 1996). For large spirals, the total stellar mass was further scaled by the galaxy’s disk/(bulge+disk) luminosity ratio from the literature to avoid representing stellar mass in the bulge with the SFH of the disk.

For the largest ANGST galaxies, most of the young (<2 Gyr) populations are not well-mixed and are not contained within a single ANGST field. Thus our assumption that the SFH in the deepest field (which is located in the outer regions of the disk, where crowding is minimized) is representative of the entire galaxy is not valid at recent timescales that do not allow sufficient radial mixing. In these cases, we therefore made use of shallower tilings that covered at least half of the optical disk. Where possible (M81, NGC 253, NGC 55, and NGC 3109), we measured the recent SFHs (<2 Gyr; $z < 0.2$) from the shallower galaxy tilings. These tilings cover the full extent of the optical disk of M81 and half of the optical disk of the other 3 galaxies (stepping along the major axis from the center). This method provides a more realistic total recent SFH for these large disk galaxies, requiring less scaling. The case of M81 required no scaling, and the other 3 galaxies required scaling only by a factor of 2 to account for the ANGST coverage. However, since a significant amount of star formation may be in unresolved clusters of stars and extinguished by dust, we still likely miss some fraction of the most recent star formation. We verified that the recent SFRs obtained by this method were at least equal to the rates that would have come out of scaling the SFH of the deep field by the total *Spitzer* stellar mass of the galaxy in order to be sure that using the shallow tiled data was, at the very least, not reducing the amount recent star formation contained in these galaxies.

We note our measuring technique is not sensitive to the stellar populations in bulges. Because of severe crowding in the central portions of the large galaxies, the pho-

tometry was too shallow to produce reliable SFHs, and was therefore not included. The galaxy most strongly under-represented due to this bias against bulges is M82, which is known to have a total current SFR $\sim 1\text{--}6 M_{\odot} \text{ yr}^{-1}$ (Young et al. 1996; Bell & Kennicutt 2001; Kennicutt et al. 2003), mainly in the central 500 pc of the galaxy. On the other hand, the disk has a recent (<40 Myr) SFR in our measurement of just $0.2 \pm 0.1 M_{\odot} \text{ yr}^{-1}$. Our measured rate is similar whether we scale the SFR as determined from our deepest data or sum the recent SFRs from the available tilings. The star formation is mainly in the bulge, which dominates the galaxy luminosity ($L_{disk}/L_{bulge} \sim 0.4$ Ichikawa et al. 1995). For this reason, ρ_{SFR} for our most recent time bin is likely only a lower limit. In NGC 253, where the star formation is more widespread throughout the disk, and the disk dominates the light ($L_{disk}/L_{bulge} \sim 4$ Simien & de Vaucouleurs 1986), our technique recovered the recent SF better. The current rate is $\sim 0.7 M_{\odot} \text{ yr}^{-1}$ (Young et al. 1996), and we measure $0.4 \pm 0.05 M_{\odot} \text{ yr}^{-1}$ (20–80 Myr). This value increases to $0.8 \pm 0.1 M_{\odot} \text{ yr}^{-1}$ when renormalized to a Salpeter IMF.

When combining these final SFHs for the sample volume, we added uncertainties in quadrature and increased the total uncertainty by a factor of $\sqrt{2}$ to approximately account for additional uncertainty from scaling and combining SFHs. We also derived total SFRs excluding M81 or NGC 253 to assess the sensitivity of our total to these massive galaxies. While this test removed a significant fraction of the total stellar mass, the SFH remained essentially unchanged in shape. However, as shown in Figure 2, M82 is disproportionately responsible for the high SFR $\sim 1\text{--}4$ Gyr ago.

3. RESULTS

Our volume-limited $\rho_{SFR}(t)$, along with the contributions of some major components (spirals, dwarfs, M81, and NGC253), is shown in Figures 2 and 3. Overall, $\rho_{SFR}(t)$ in the local volume is clearly dominated by that of the large spirals NGC 253 and M81. In Figure 4, we plot $\rho_{SFR}(t)$, scaled to match the cosmic mean stellar density, along with a compilation of literature studies (Hopkins 2004, 2007; Reddy et al. 2008; Heavens et al. 2004), the LG (Drozdosvsky et al. 2008), and two theoretical results (Lacey et al. 2009; Springel & Hernquist 2003). The models are not easily compared to our results because most of our time resolution comes at epochs more recent than $z = 1$ whereas the models typically provide one data point per unit redshift. However, overall it is encouraging that our results are similar to the observational results already in the literature, determined using other techniques, that our results are similar to the SFH of the LG, and that our results fall within the wide range of theoretical calculations. We note that our result differs from those of Heavens et al. (2004), which analyzed spectra of $\sim 10^5$ nearby galaxies and found the local $\rho_{SFR}(t)$ peak at $z \sim 0.6$. While both measurements show enhanced star formation at lookback times of $\sim 2\text{--}6$ Gyr, the discrepancy is in the $z > 2$ (>10 Gyr) bin, where our measured rate is a factor of 3 larger than theirs, placing our peak rate in this oldest bin. Their sample and technique remain the only ones to have measured such a low rate for $z > 2$.

Despite the diversity of SFHs in local dwarf galaxies ($M_B > -18$ Weisz et al 2011a), when one sums their total $\rho_{SFR}(t)$, it is remarkably similar to that of the full galaxy sample prior to $z \sim 0.1$ (>1 Gyr lookback time). For all but this recent epoch, the $\rho_{SFR}(t)$ pattern for the dwarfs is indistinguishable from that of the large spirals, which, in turn, is indistinguishable from that of the sample volume. Therefore, we do not detect any significant difference between the formation times of dwarf galaxies and large spirals, suggesting that any differences occurred prior to $z \sim 2$ (>10 Gyr ago).

At lookback times $\gtrsim 4$ Gyr ($z \gtrsim 0.5$), our total SFRs are indistinguishable from those of most redshift surveys. However, our recent SFRs are higher than those of redshift surveys, similar to those of the LG (Drozdosky et al. 2008). This result is largely due to our inclusion of low-mass galaxies (other spirals and dwarfs in Figures 2 and 3), which contribute 50% of the SFR at recent times. Such low-mass galaxies are typically not included in redshift surveys due to their low luminosities.

4. CONCLUSIONS

We have derived $\rho_{SFR}(t)$ for galaxy disks in our local volume using resolved stellar photometry. This measurement includes the contribution by different galaxy types. Our sample is dominated, in number, by galaxies fainter than the limits of any available redshift survey or high- z *HST* imaging. Thus, our $\rho_{SFR}(t)$ represents a portion of parameter space not yet studied in detail outside the LG. However, our sample is lacking in massive spheroids, whose mean $\rho_{SFR}(t)$ is more reliably determined from

the large samples included in redshift surveys and high- z *HST* imaging.

We find that, while $\rho_{SFR}(t)$ is dominated by that of the spirals, the overall shape of the measurement is robust against removal of any single galaxy. We also find that the combined $\rho_{SFR}(t)$ of the dwarf galaxies is not significantly different in shape from that of the larger spirals except for the most recent Gyr, suggesting that $\sim 50\%$ of the stellar mass in both types of systems formed prior to $z \sim 2$. This result is consistent with those of Thomas et al. (2005) for high-density environments.

We have compared our measurements to those obtained by galaxy surveys and analysis of the HDF and UDF. We find overall agreement between our results and those of galaxy surveys; however, our measurements do not yet have the time resolution at epochs prior to 10 Gyr ($z \gtrsim 2$) to resolve the peak in cosmic SFR density. Our measurements suggest that this peak lies prior to $z \sim 2$, consistent with the most recent *HST/WFC3* results, which place the peak at $z \sim 4$ (Bouwens et al. 2010). Finally, at recent times, the contribution of low-mass galaxies to the total SFR has increased, resulting in a higher total rate at recent times than observed by other methods.

Support for this work was provided by NASA through grants GO-10915, GO-11986, and Hubble Fellowship grant (for KMG) HST-HF-51273.01 awarded by the Space Telescope Science Institute, which is operated by the Association of Universities for Research in Astronomy, Inc., for NASA, under contract NAS 5-26555.

REFERENCES

- Adler, D. S., & Westpfahl, D. J. 1996, *AJ*, 111, 735
 Bell, E. F., & Kennicutt, R. C., Jr. 2001, *ApJ*, 548, 681
 Bouwens, R. J., Illingworth, G. D., Franx, M., & Ford, H. 2007, *ApJ*, 670, 928
 Bouwens, R. J., et al. 2010, *ApJ*, 709, L133
 Bunker, A. J., Stanway, E. R., Ellis, R. S., & McMahon, R. G. 2004, *MNRAS*, 355, 374
 Chapman, S. C., Blain, A. W., Smail, I., & Ivison, R. J. 2005, *ApJ*, 622, 772
 Connolly, A. J., Szalay, A. S., Dickinson, M., Subbarao, M. U., & Brunner, R. J. 1997, *ApJ*, 486, L11
 Cowie, L. L., Songaila, A., Hu, E. M., & Cohen, J. G. 1996, *AJ*, 112, 839
 Dalcanton, J. J., et al. 2009, *ApJS*, 183, 67
 Dale, D. A., et al. 2009, *ApJ*, 703, 517
 Dolphin, A. E. 2000, *PASP*, 112, 1383
 Dolphin, A. E. 2002, *MNRAS*, 332, 91
 Drozdovsky, I., Hopkins, A., Aparicio, A., & Gallart, C. 2008, *Matching the Local and Cosmic Star Formation Histories*, ed. Koribalski, B. S. & Jerjen, H. (Springer Netherlands), 143
 Dunkley, J., et al. 2009, *ApJS*, 180, 306
 Fontana, A., Poli, F., Menci, N., Nonino, M., Giallongo, E., Cristiani, S., & D'Odorico, S. 2003, *ApJ*, 587, 544
 Gallart, C., Zoccali, M., & Aparicio, A. 2005, *ARA&A*, 43, 387
 Giallisco, M., et al. 2004, *ApJ*, 600, L103
 Girardi, L., Bertelli, G., Bressan, A., Chiosi, C., Groenewegen, M. A. T., Marigo, P., Salasnich, B., & Weiss, A. 2002, *A&A*, 391, 195
 Girardi, L., et al. 2010, *ApJ*, submitted
 Heavens, A., Panter, B., Jimenez, R., & Dunlop, J. 2004, *Nature*, 428, 625
 Hernquist, L., & Springel, V. 2003, *MNRAS*, 341, 1253
 Holtzman, J., Dalcanton, D., J.J. Garnett, Sarajedini, A., & Williams, B. F. 2009, *AJ*, submitted
 Hopkins, A. M. 2004, *ApJ*, 615, 209
 Hopkins, A. M. 2007, *ApJ*, 654, 1175
 Hopkins, A. M., Irwin, M. J., & Connolly, A. J. 2001, *ApJ*, 558, L31
 Ichikawa, T., Yanagisawa, K., Itoh, N., Tarusawa, K., van Driel, W., & Ueno, M. 1995, *AJ*, 109, 2038
 Iwata, I., Ohta, K., Tamura, N., Ando, M., Wada, S., Watanabe, C., Akiyama, M., & Aoki, K. 2003, *PASJ*, 55, 415
 Kennicutt, R. C., Jr., et al. 2003, *PASP*, 115, 928
 Kroupa, P. 2002, *Science*, 295, 82
 Lacey, C. G., Baugh, C. M., Frenk, C. S., Benson, A. J., Orsi, A., Silva, L., Granato, G. L., & Bressan, A. 2009, *ArXiv e-prints*
 Lanzetta, K. M., Yahata, N., Pascarelle, S., Chen, H., & Fernández-Soto, A. 2002, *ApJ*, 570, 492
 Lilly, S. J., Carollo, C. M., & Stockton, A. N. 2003, *ApJ*, 597, 730
 Lilly, S. J., Le Fevre, O., Hammer, F., & Crampton, D. 1996, *ApJ*, 460, L1
 Madau, P., Ferguson, H. C., Dickinson, M. E., Giallisco, M., Steidel, C. C., & Fruchter, A. 1996, *MNRAS*, 283, 1388
 Marigo, P., Girardi, L., Bressan, A., Groenewegen, M. A. T., Silva, L., & Granato, G. L. 2008, *A&A*, 482, 883
 Melbourne, J., Williams, B., Dalcanton, J., Ammons, S. M., Max, C., Koo, D. C., Girardi, L., & Dolphin, A. 2010, *ApJ*, 712, 469
 Neistein, E., van den Bosch, F. C., & Dekel, A. 2006, *MNRAS*, 372, 933
 Puche, D., Carignan, C., & van Gorkom, J. H. 1991, *AJ*, 101, 456
 Reddy, N. A., Steidel, C. C., Pettini, M., Adelberger, K. L., Shapley, A. E., Erb, D. K., & Dickinson, M. 2008, *ApJS*, 175, 48
 Salpeter, E. E. 1955, *ApJ*, 121, 161
 Schiminovich, D., et al. 2005, *ApJ*, 619, L47
 Simien, F., & de Vaucouleurs, G. 1986, *ApJ*, 302, 564
 Springel, V., & Hernquist, L. 2003, *MNRAS*, 339, 312
 Steidel, C. C., Adelberger, K. L., Giallisco, M., Dickinson, M., & Pettini, M. 1999, *ApJ*, 519, 1
 Thomas, D., Maraston, C., Bender, R., & Mendes de Oliveira, C. 2005, *ApJ*, 621, 673
 van den Bergh, S. 2000, *PASP*, 112, 529

Weisz, D. R., et al. 2011a, arXiv:1101.1093
Weisz, D. R., et al. 2011b, arXiv:1101.1301
Williams, B. F., et al. 2009, AJ, 137, 419

Young, J. S., Allen, L., Kenney, J. D. P., Lesser, A., & Rownd, B.
1996, AJ, 112, 1903

TABLE 1
DATA USED FOR SFH DETERMINATION

Galaxy	Proposal	Target	Camera	Filter	Exposure (s)	Stars	$m_{50\%}$	$M_{50\%}$
Antlia/P29194	10210	ANTLIA	ACS	F606W	985	19226	28.01	2.18
Antlia/P29194	10210	ANTLIA	ACS	F814W	1174	19226	27.30	1.54
KK230	9771	KK230	ACS	F606W	1200	4679	28.15	1.69
KK230	9771	KK230	ACS	F814W	900	4679	27.08	0.64
E410-005/KK3	10503	ESO410-005	ACS	F606W	8960	79952	28.85	2.39
E410-005/KK3	10503	ESO410-005	ACS	F814W	22400	79952	27.92	1.48
E294-010	10503	ESO294-010	ACS	F606W	13920	103465	28.95	2.52
E294-010	10503	ESO294-010	ACS	F814W	27840	103465	28.51	2.08
GR8/DDO155	10915	GR8	ACS	F475W	2244	22134	28.23	1.52
GR8/DDO155	10915	GR8	ACS	F814W	2259	22134	27.46	0.80
N300	10915	NGC0300-WIDE1	ACS	F606W	1515	224152	27.89	1.19
N300	10915	NGC0300-WIDE1	ACS	F814W	1542	224152	27.00	0.31
DDO187	10210	UGC9128	ACS	F606W	985	27599	27.88	1.02
DDO187	10210	UGC9128	ACS	F814W	1174	27599	27.13	0.30
KKH98	10915	KKH98	ACS	F475W	2265	10904	28.21	0.78
KKH98	10915	KKH98	ACS	F814W	2280	10904	27.41	0.22
U8508	10915	UGC8508	ACS	F475W	2280	45958	27.97	0.87
U8508	10915	UGC8508	ACS	F814W	2349	45958	27.32	0.25
DDO190/U9240	10915	DDO190	ACS	F606W	2301	105910	28.15	0.89
DDO190/U9240	10915	DDO190	ACS	F814W	2265	105910	27.35	0.10
DDO113/KDG90	10915	DDO113	ACS	F475W	2265	21150	28.21	0.85
DDO113/KDG90	10915	DDO113	ACS	F814W	2280	21150	27.43	0.11
DDO181/U8651	10210	UGC8651	ACS	F606W	1016	41855	27.96	0.54
DDO181/U8651	10210	UGC8651	ACS	F814W	1209	41855	27.12	-0.29
N3741	10915	NGC3741	ACS	F475W	2262	29476	28.04	0.54
N3741	10915	NGC3741	ACS	F814W	2331	29476	27.33	-0.12
N4163	10915	NGC4163	ACS	F606W	2292	97632	28.05	0.63
N4163	10915	NGC4163	ACS	F814W	2250	97632	27.32	-0.08
UA292	10915	UGCA292	ACS	F606W	926	8913	27.89	0.39
UA292	10915	UGCA292	ACS	F814W	2274	8913	27.39	-0.10
U8833	10210	UGC8833	ACS	F606W	998	19438	27.89	0.39
U8833	10210	UGC8833	ACS	F814W	1189	19438	27.11	-0.38
DDO183/U8760	10210	UGC8760	ACS	F606W	998	36852	27.86	0.30
DDO183/U8760	10210	UGC8760	ACS	F814W	1189	36852	27.08	-0.46
N2366	10605	NGC-2366-2	ACS	F555W	4780	237638	28.06	0.41
N2366	10605	NGC-2366-2	ACS	F814W	4780	237638	27.53	-0.06
DDO44/KK61	10915	DDO44	ACS	F475W	2361	34481	28.31	0.62
DDO44/KK61	10915	DDO44	ACS	F814W	2430	34481	27.55	-0.06
DDO6	10915	DDO6	ACS	F475W	2250	23799	28.34	0.66
DDO6	10915	DDO6	ACS	F814W	2268	23799	27.53	-0.12
KKH37/Mai16	10915	KKH37	ACS	F475W	2469	15361	28.31	0.36
KKH37/Mai16	10915	KKH37	ACS	F814W	2541	15361	27.58	-0.22
HoII/DDO50	10605	UGC-4305-1	ACS	F555W	4660	248011	27.95	0.19
HoII/DDO50	10605	UGC-4305-1	ACS	F814W	4660	248011	27.38	-0.33
KDG2/E540-030	10503	ESO540-030	ACS	F606W	6720	16964	28.67	0.94
KDG2/E540-030	10503	ESO540-030	ACS	F814W	6720	16964	27.81	0.11
E540-032/FG24	10503	ESO540-032	ACS	F606W	8960	34278	28.87	1.14
E540-032/FG24	10503	ESO540-032	ACS	F814W	4480	34278	27.72	0.01
FM1	9884	M81F6D1	ACS	F606W	17200	19373	28.86	0.98
FM1	9884	M81F6D1	ACS	F814W	9000	19373	27.79	-0.02
KK77	9884	M81F12D1	ACS	F606W	17200	59039	29.06	0.93
KK77	9884	M81F12D1	ACS	F814W	9000	59039	27.98	-0.01
KDG63/KK83	9884	DDO71	ACS	F606W	17200	57133	28.92	0.92
KDG63/KK83	9884	DDO71	ACS	F814W	9000	57133	28.01	0.10
M82	10776	M82-POS4	ACS	F555W	1360	31842	27.29	-0.51
M82	10776	M82-POS4	ACS	F814W	700	31842	26.35	-1.43
KDG52	10605	MESSIER-081-DWARF-A	ACS	F555W	5914	20335	28.54	0.72
KDG52	10605	MESSIER-081-DWARF-A	ACS	F814W	5936	20335	27.99	0.20
DDO53	10605	UGC-04459	ACS	F555W	4768	80038	28.32	0.44
DDO53	10605	UGC-04459	ACS	F814W	4768	80038	27.76	-0.07
N2976	10915	NGC2976-DEEP	ACS	F606W	18716	105537	29.21	1.25
N2976	10915	NGC2976-DEEP	ACS	F814W	27091	105537	28.59	0.70
KDG61/KK81	9884	M81K61	ACS	F606W	17200	80746	29.06	1.07
KDG61/KK81	9884	M81K61	ACS	F814W	9000	80746	28.10	0.18
M81	10915	M81-DEEP	ACS	F606W	24132	171101	29.69	1.65
M81	10915	M81-DEEP	ACS	F814W	29853	171101	29.04	1.08
M81	10584	M81-FIELD-10	ACS	F435W	1200	23950	27.49	-0.68
M81	10584	M81-FIELD-10	ACS	F606W	1200	23950	27.35	-0.69
M81	10584	M81-FIELD-11	ACS	F435W	1200	64029	27.43	-0.74
M81	10584	M81-FIELD-11	ACS	F606W	1200	64029	27.18	-0.86
M81	10584	M81-FIELD-12	ACS	F435W	1200	94882	27.17	-1.00
M81	10584	M81-FIELD-12	ACS	F606W	1200	94882	26.63	-1.41
M81	10584	M81-FIELD-13	ACS	F435W	1200	100833	27.21	-0.96
M81	10584	M81-FIELD-13	ACS	F606W	1200	100833	26.75	-1.29
M81	10584	M81-FIELD-14	ACS	F435W	1200	45241	27.51	-0.66

TABLE 1 — *Continued*

Galaxy	Proposal	Target	Camera	Filter	Exposure (s)	Stars	$m_{50\%}$	$M_{50\%}$
M81	10584	M81-FIELD-14	ACS	F606W	1200	45241	27.31	-0.73
M81	10584	M81-FIELD-15	ACS	F435W	1200	48611	27.38	-0.79
M81	10584	M81-FIELD-15	ACS	F606W	1200	48611	27.21	-0.83
M81	10584	M81-FIELD-16	ACS	F435W	1200	117652	26.93	-1.24
M81	10584	M81-FIELD-16	ACS	F606W	1200	117652	26.40	-1.64
M81	10584	M81-FIELD-17	ACS	F435W	1200	121280	27.12	-1.05
M81	10584	M81-FIELD-17	ACS	F606W	1200	121280	26.43	-1.61
M81	10584	M81-FIELD-18	ACS	F435W	1200	71571	27.39	-0.78
M81	10584	M81-FIELD-18	ACS	F606W	1200	71571	27.19	-0.85
M81	10584	M81-FIELD-19	ACS	F435W	1200	46894	27.46	-0.71
M81	10584	M81-FIELD-19	ACS	F606W	1200	46894	27.12	-0.92
M81	10584	M81-FIELD-20	ACS	F435W	1200	73703	27.28	-0.89
M81	10584	M81-FIELD-20	ACS	F606W	1200	73703	26.91	-1.13
M81	10584	M81-FIELD-21	ACS	F435W	1200	68639	27.26	-0.91
M81	10584	M81-FIELD-21	ACS	F606W	1200	68639	26.88	-1.16
M81	10584	M81-FIELD-22	ACS	F435W	1200	28694	27.56	-0.61
M81	10584	M81-FIELD-22	ACS	F606W	1200	28694	27.39	-0.65
M81	10584	M81-FIELD-23	ACS	F435W	1200	27768	27.61	-0.56
M81	10584	M81-FIELD-23	ACS	F606W	1200	27768	27.46	-0.58
M81	10584	M81-FIELD-24	ACS	F435W	1200	65533	27.48	-0.69
M81	10584	M81-FIELD-24	ACS	F606W	1200	65533	27.30	-0.74
M81	10584	M81-FIELD-25	ACS	F435W	1200	66310	27.43	-0.74
M81	10584	M81-FIELD-25	ACS	F606W	1200	66310	27.21	-0.83
M81	10584	M81-FIELD-26	ACS	F435W	1200	13063	27.65	-0.52
M81	10584	M81-FIELD-26	ACS	F606W	1200	13063	27.36	-0.68
M81	10584	M81-FIELD-27	ACS	F606W	1580	136043	27.99	-0.05
M81	10584	M81-FIELD-27	ACS	F814W	1595	136043	27.20	-0.76
M81	10584	M81-FIELD-28	ACS	F606W	1580	190198	27.96	-0.08
M81	10584	M81-FIELD-28	ACS	F814W	1595	190198	27.18	-0.78
M81	10584	M81-FIELD-29	ACS	F606W	1580	80855	28.05	0.01
M81	10584	M81-FIELD-29	ACS	F814W	1595	80855	27.25	-0.71
M81	10584	M81-FIELD-1	ACS	F606W	1580	84484	28.01	-0.03
M81	10584	M81-FIELD-1	ACS	F814W	1595	84484	27.16	-0.80
M81	10584	M81-FIELD-2	ACS	F606W	1580	119880	28.03	-0.01
M81	10584	M81-FIELD-2	ACS	F814W	1595	119880	27.17	-0.79
M81	10584	M81-FIELD-3	ACS	F435W	1200	12807	27.59	-0.58
M81	10584	M81-FIELD-3	ACS	F606W	1200	12807	27.53	-0.51
M81	10584	M81-FIELD-4	ACS	F435W	1200	42770	27.48	-0.69
M81	10584	M81-FIELD-4	ACS	F606W	1200	42770	27.39	-0.65
M81	10584	M81-FIELD-5	ACS	F435W	1200	57981	27.49	-0.68
M81	10584	M81-FIELD-5	ACS	F606W	1200	57981	27.37	-0.67
M81	10584	M81-FIELD-6	ACS	F435W	1200	19856	27.61	-0.56
M81	10584	M81-FIELD-6	ACS	F606W	1200	19856	27.33	-0.71
M81	10584	M81-FIELD-7	ACS	F435W	1200	25584	27.51	-0.66
M81	10584	M81-FIELD-7	ACS	F606W	1200	25584	27.34	-0.70
M81	10584	M81-FIELD-8	ACS	F435W	1200	120790	27.37	-0.80
M81	10584	M81-FIELD-8	ACS	F606W	1200	120790	26.99	-1.05
M81	10584	M81-FIELD-9	ACS	F435W	1200	103540	27.32	-0.85
M81	10584	M81-FIELD-9	ACS	F606W	1200	103540	27.05	-0.99
N247	10915	NGC0247-WIDE1	ACS	F606W	2280	193431	28.01	0.14
N247	10915	NGC0247-WIDE1	ACS	F814W	2250	193431	27.23	-0.62
HoIX/DDO66	10605	UGC-5336	ACS	F555W	4768	57610	28.44	0.32
HoIX/DDO66	10605	UGC-5336	ACS	F814W	4768	57610	27.91	-0.09
KDG64/KK85	9884	M81K64	ACS	F606W	17200	68420	29.19	1.18
KDG64/KK85	9884	M81K64	ACS	F814W	9000	68420	28.35	0.40
IKN	9771	IKN	ACS	F606W	1200	24626	28.03	-0.22
IKN	9771	IKN	ACS	F814W	900	24626	26.95	-1.16
DDO78/KK89	10915	DDO78	ACS	F475W	2274	36430	28.19	0.23
DDO78/KK89	10915	DDO78	ACS	F814W	2292	36430	27.54	-0.37
N3077	10915	NGC3077-WIDE1	ACS	F606W	1596	442068	26.84	-1.27
N3077	10915	NGC3077-WIDE1	ACS	F814W	1622	442068	26.34	-1.70
HoI/DDO63	10605	UGC-5139	ACS	F555W	4446	123920	28.34	0.25
HoI/DDO63	10605	UGC-5139	ACS	F814W	5936	123920	27.88	-0.14
A0952+69	10915	A0952	ACS	F475W	2250	7810	28.42	0.15
A0952+69	10915	A0952	ACS	F814W	2265	7810	27.63	-0.48
N253	10523	NGC0253-HALO-2	ACS	F606W	680	11830	27.56	-0.47
N253	10523	NGC0253-HALO-2	ACS	F814W	680	11830	26.66	-1.35
N253	10523	NGC0253-HALO-11	ACS	F606W	680	27423	27.47	-0.56
N253	10523	NGC0253-HALO-11	ACS	F814W	680	27423	26.57	-1.44
N253	10523	NGC0253-HALO-12	ACS	F606W	680	8326	27.70	-0.33
N253	10523	NGC0253-HALO-12	ACS	F814W	680	8326	26.73	-1.28
N253	10523	NGC0253-HALO-17	ACS	F606W	680	62499	27.62	-0.41
N253	10523	NGC0253-HALO-17	ACS	F814W	680	62499	26.68	-1.33
N253	10523	NGC0253-HALO-18	ACS	F606W	680	42574	27.62	-0.41
N253	10523	NGC0253-HALO-18	ACS	F814W	680	42574	26.62	-1.39
N253	10915	NGC0253-WIDE1	ACS	F606W	2283	293299	28.04	0.01

TABLE 1 — *Continued*

Galaxy	Proposal	Target	Camera	Filter	Exposure (s)	Stars	$m_{50\%}$	$M_{50\%}$
N253	10915	NGC0253-WIDE1	ACS	F814W	2253	293299	27.26	-0.75
N253	10915	NGC0253-WIDE2	ACS	F606W	1508	435333	27.21	-0.82
N253	10915	NGC0253-WIDE2	ACS	F814W	1534	435333	26.50	-1.51
N253	10915	NGC0253-WIDE3	ACS	F606W	1508	427307	26.52	-1.51
N253	10915	NGC0253-WIDE3	ACS	F814W	1534	427307	25.79	-2.22
N253	10915	NGC0253-WIDE4	ACS	F606W	1508	417964	26.13	-1.90
N253	10915	NGC0253-WIDE4	ACS	F814W	1534	417964	25.32	-2.69
N253	10915	NGC0253-WIDE5	ACS	F606W	1508	348456	25.66	-2.37
N253	10915	NGC0253-WIDE5	ACS	F814W	1534	348456	24.46	-3.55
HS117	9771	HS117	ACS	F606W	1200	7317	28.01	-0.31
HS117	9771	HS117	ACS	F814W	900	7317	27.05	-1.16
DDO82	10915	DDO82	ACS	F606W	2454	172885	28.13	-0.01
DDO82	10915	DDO82	ACS	F814W	2442	172885	27.46	-0.64
BK3N	10915	BK3N	ACS	F475W	2250	8164	28.40	0.06
BK3N	10915	BK3N	ACS	F814W	2265	8164	27.58	-0.60
I2574	9755	IC2574-SGS	ACS	F555W	6400	342454	28.14	-0.01
I2574	9755	IC2574-SGS	ACS	F814W	6400	342454	27.62	-0.47
SexA/DDO75	7496	DDO75	WFPC2	F555W	19200	33295	27.37	1.62
SexA/DDO75	7496	DDO75	WFPC2	F814W	38400	33295	26.63	0.94
N3109	10915	NGC3109-DEEP	WFPC2	F606W	2700	13262	26.75	0.93
N3109	10915	NGC3109-DEEP	WFPC2	F814W	3900	13262	26.00	0.25
N3109	11307	NGC3109-WIDE1	WFPC2	F606W	2700	21710	26.84	1.02
N3109	11307	NGC3109-WIDE1	WFPC2	F814W	3900	21710	25.85	0.10
N3109	11307	NGC3109-WIDE2	WFPC2	F606W	2700	30297	26.73	0.91
N3109	11307	NGC3109-WIDE2	WFPC2	F814W	3900	30297	25.76	0.01
N3109	11307	NGC3109-WIDE3	WFPC2	F606W	2400	34166	26.52	0.70
N3109	11307	NGC3109-WIDE3	WFPC2	F814W	2400	34166	25.47	-0.28
N3109	11307	NGC3109-WIDE4	WFPC2	F606W	2400	42509	26.11	0.29
N3109	11307	NGC3109-WIDE4	WFPC2	F814W	2400	42509	25.26	-0.49
SexB/DDO70	10915	SEXB-DEEP	WFPC2	F606W	2700	29624	26.75	0.99
SexB/DDO70	10915	SEXB-DEEP	WFPC2	F814W	3900	29624	25.92	0.19
KKR25	8601	KKR25	WFPC2	F606W	600	923	26.13	-0.24
KKR25	8601	KKR25	WFPC2	F814W	600	923	24.98	-1.39
I5152/E237-27	10915	IC5152-DEEP	WFPC2	F606W	4800	325	27.32	0.67
I5152/E237-27	10915	IC5152-DEEP	WFPC2	F814W	9600	325	26.45	-0.18
N55	11307	NGC0055-WIDE1	WFPC2	F606W	2000	37013	26.61	-0.06
N55	11307	NGC0055-WIDE1	WFPC2	F814W	3700	37013	25.74	-0.92
N55	11307	NGC0055-WIDE2	WFPC2	F606W	1800	36771	26.41	-0.26
N55	11307	NGC0055-WIDE2	WFPC2	F814W	2600	36771	25.56	-1.10
N55	11307	NGC0055-WIDE3	WFPC2	F606W	2700	47212	26.01	-0.66
N55	11307	NGC0055-WIDE3	WFPC2	F814W	3900	47212	25.25	-1.41
N55	11307	NGC0055-WIDE4	WFPC2	F606W	2700	55453	25.58	-1.09
N55	11307	NGC0055-WIDE4	WFPC2	F814W	3900	55453	24.84	-1.82
N55	11307	NGC0055-WIDE5	WFPC2	F606W	2700	54136	25.55	-1.12
N55	11307	NGC0055-WIDE5	WFPC2	F814W	3900	54136	24.73	-1.93
N55	10915	NGC0055-DEEP	WFPC2	F606W	6000	17055	27.50	0.83
N55	10915	NGC0055-DEEP	WFPC2	F814W	10800	17055	26.69	0.03
UA438	8192	E407-G18	WFPC2	F606W	600	5016	26.04	-0.74
UA438	8192	E407-G18	WFPC2	F814W	600	5016	24.97	-1.80
DDO125/U7577	8601	UGC7577	WFPC2	F606W	600	11520	26.02	-1.07
DDO125/U7577	8601	UGC7577	WFPC2	F814W	600	11520	24.91	-2.15
KKH86	8601	KKH71	WFPC2	F606W	600	727	26.19	-0.97
KKH86	8601	KKH71	WFPC2	F814W	600	727	25.08	-2.06
DDO99/U6817	8601	UGC6817	WFPC2	F606W	600	6536	26.13	-1.05
DDO99/U6817	8601	UGC6817	WFPC2	F814W	600	6536	24.98	-2.18
N4214	10915	NGC4214-DEEP	WFPC2	F606W	15600	16806	27.97	0.57
N4214	10915	NGC4214-DEEP	WFPC2	F814W	31200	16806	27.20	-0.18
N404	10915	NGC0404-DEEP	WFPC2	F606W	39000	40793	27.25	-0.35
N404	10915	NGC0404-DEEP	WFPC2	F814W	75400	40793	26.76	-0.78
E321-014	8601	PGC39032	WFPC2	F606W	600	1745	25.98	-1.81
E321-014	8601	PGC39032	WFPC2	F814W	600	1745	24.91	-2.79
U4483	8769	UGC4483	WFPC2	F555W	9500	6634	27.67	0.02
U4483	8769	UGC4483	WFPC2	F814W	6900	6634	26.37	-1.23
N4190	10905	NGC-4190	WFPC2	F606W	2200	12549	26.74	-1.07
N4190	10905	NGC-4190	WFPC2	F814W	2200	12549	25.46	-2.32
F8D1	5898	GAL-094447+672619	WFPC2	F555W	9000	14226	27.84	-0.37
F8D1	5898	GAL-094447+672619	WFPC2	F814W	15200	14226	27.05	-1.02
BK5N	6964	GAL-100441+681522	WFPC2	F555W	15600	2332	27.78	-0.31
BK5N	6964	GAL-100441+681522	WFPC2	F814W	21340	2332	26.95	-1.05
N2403	10915	NGC2403-DEEP	WFPC2	F606W	32400	30617	28.05	0.34
N2403	10915	NGC2403-DEEP	WFPC2	F814W	62100	30617	27.20	-0.47
MCG9-20-131	11986	MCG9-20-131	WFPC2	F606W	10700	9088	27.89	0.01
MCG9-20-131	11986	MCG9-20-131	WFPC2	F814W	19300	9088	26.82	-1.12

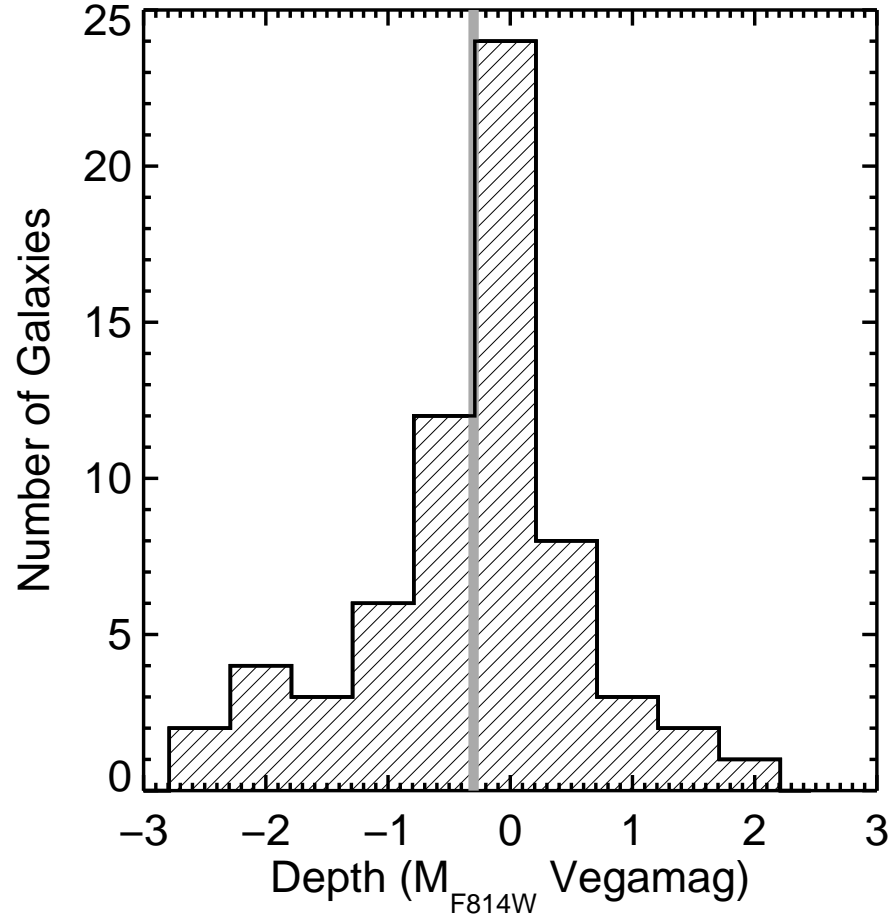


FIG. 1.— Histogram of the 50% completeness limiting F814W absolute magnitude for the sample galaxies. These values have been corrected for distance and extinction. The depth of 58% is fainter than the red clump in our M81 data (thick gray line).

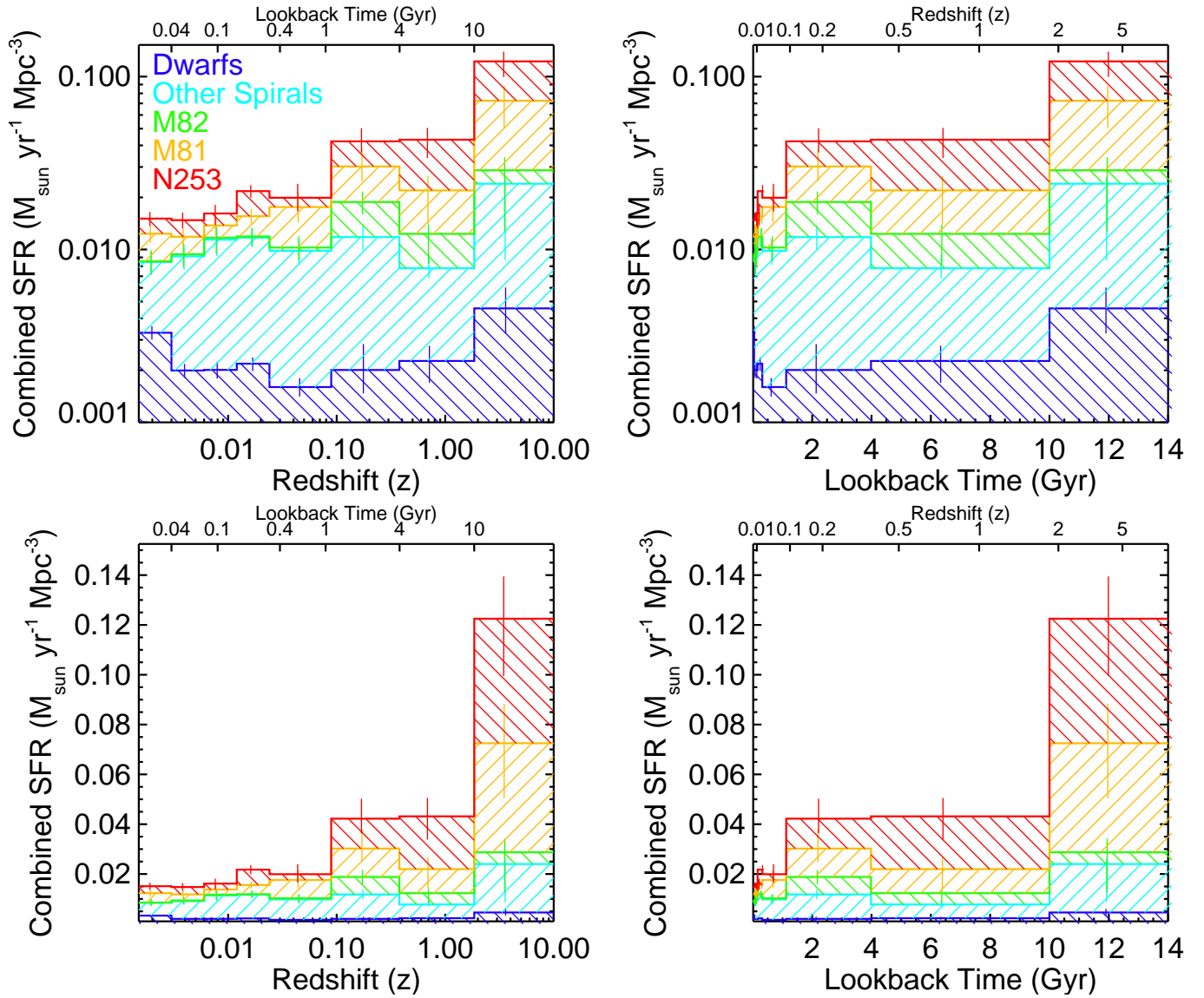


FIG. 2.— *Top Left*: The SFR density of the local volume. Error bars show the scaled root-sum-squared of the uncertainty estimates from our measured SFHs (§ 2.1). Histograms denote combined $\rho_{SFR}(t)$ including all 54 dwarf galaxies in the sample (blue), 8 of the spiral disks (all but M82, M81, and NGC 253), M82 alone (green), M81 alone (yellow) and, completing the sample, NGC 253 alone (red). *Other Panels*: Same as *Top Left* but with linear lookback time (top right), linear SFR (bottom left), and both (bottom right). We adopt a five-year WMAP (Dunkley et al. 2009) cosmology for all conversions between time and redshift.

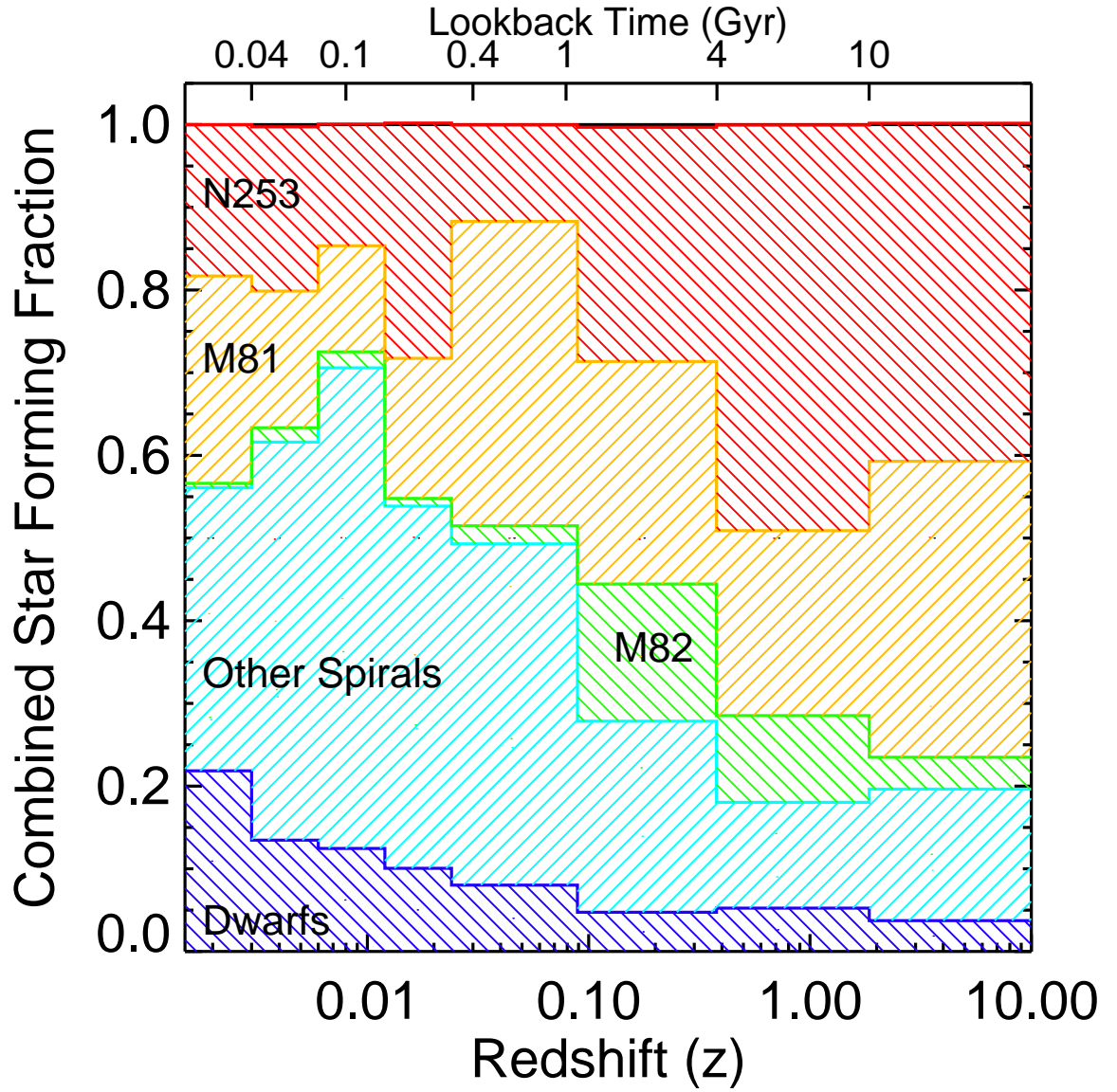


FIG. 3.— Fractional contribution of several components to the total SFH of the survey volume. Colors are the same as in Figure 2.

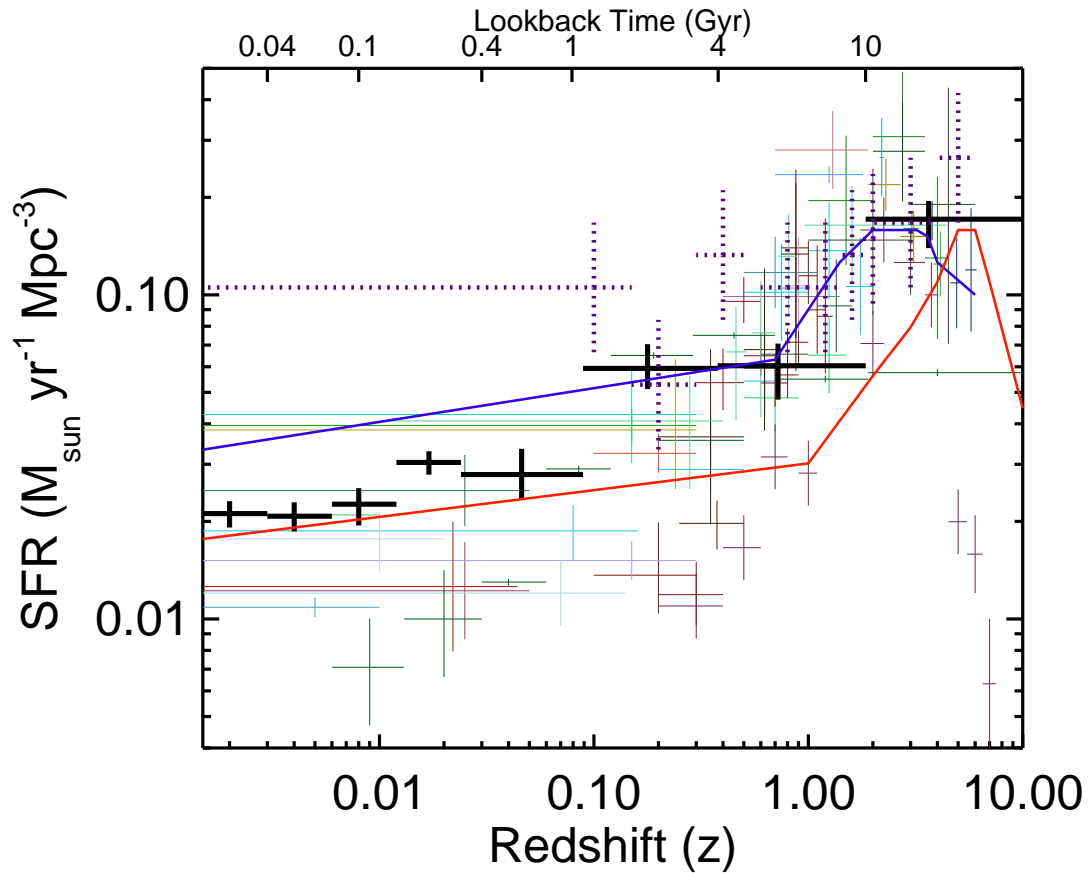


FIG. 4.— *Black Error Bars:* $\rho_{SFR}(t)$ measured from the ANGST sample. Values have been scaled to reproduce the mean cosmic stellar density for relevant comparison. *Color Error Bars:* Measurements taken from the compilation of Hopkins (2004) with updates included in Hopkins (2007) and the results of Heavens et al. (2004), Reddy et al. (2008), and Bouwens et al. (2010). *Dotted Error Bars:* Measurements taken from the LG study of Drozdovsky et al. (2008), scaled by a factor of 3 to compensate for the overdensity of the LG. *Lines:* Theoretical predictions from semi-analytic galaxy evolution calculations (blue, Lacey et al. 2009) and hydrodynamic simulations (Springel & Hernquist 2003, red.).